Available online at http://scik.org

J. Math. Comput. Sci. 11 (2021), No. 4, 4395-4410

https://doi.org/10.28919/jmcs/5870

ISSN: 1927-5307

DUAL BAND DIELECTRIC RESONATOR ANTENNA FOR HIGH-SPEED APPLICATIONS

SOVAN MOHANTY, BAIBASWATA MOHAPATRA*

School of Electrical, Electronics and Communication Engineering, Galgotias University, Greater Noida 201310, India

Abstract: The antennas for wireless communication devices have undergone a tremendous expansion from the external monoband resonant antenna to the internal non-resonant multi-band antenna. In this paper, a dual-band dielectric resonator antenna for high-speed applications is proposed. Due to the complex edge-shaped boundary between the dielectric and air in a rectangular dielectric resonator antenna, a complex closed form of expression is difficult to achieve. To address this problem a half-cut cylinder is placed over the rectangular dielectric to achieve excellent radiation characteristics. This proposed antenna provides a wide dual-band response with fractional impedance bandwidth of 21.92% and 19.09%while operating from7.32 GHz to 9.12 GHz and 10.71 GHz to 12.95 GHz. It provides an average gain of 3dBi with high gain stability in the entire operating frequency band. The radiation efficiency is found to be 96% due to low ohmic and dielectric losses. The cross-polarization is around 20 dB lesser than the co-polarization. Its gain and directivity can further be enhanced by implementing serial and parallel array structures. This design uses HFSS 14.0 commercial electromagnetic simulation tools.

Keywords: dielectric resonator antenna; non-radiating dielectric guide; high speed communication; perfect electrical conductor.

2010 AMS Subject Classification: 68N30.

*Corresponding author

E-mail address: writetobm@gmail.com

Received April 15, 2021

1. INTRODUCTION

Wireless near field wideband communication has been undergoing tremendous growth in recent times due to the expansion of technologies like the Internet of Things (IoT), Blue tooth, Wireless Local Loop (WLL), Wireless Fidelity (Wi-Fi), Local Multipoint Distributive System (LMDS), etc. These techniques concentrate on the frequency range of 3.1 GHz to 10.6 GHz and expanded up to the X-band range. Enhancement of the data rate can be directed towards enabling existing technologies in wireless communication. There are numerous ways such as the number of independent channels can be increased to enhance the capacity. But the real challenge is to place the antenna in the right place. The proximity will degrade the MIMO advantages due to signal correlation. Implementation of advanced modulation and coding techniques along with ultra densification of the network through smaller cells improves device to device communication.

According to Shannon's first theorem for error-free high-speed communication, it is required that the rate of data transmission (R) has to be smaller than the channel capacity(C), Kraus and Fleisch[1]. From equation 1 it is found that channel capacity is correlated with the channel bandwidth and they are related to the frequency of operation. Therefore, to achieve high-speed communication the targeted technology will be microwave, millimeter-wave, and terahertz wave technologies. But random non-linearity, non-homogeneous, and non-isotropic behavior along with the effect of severe attenuation made it challenging. When the wavelength is comparable to the physical dimension of the device, effects like phase reversal and transit time effect dominates. However, in high-frequency design, the major problem comes due to variation in phase velocity w.r.t the wavelength, called dispersion, Harrington[2].

The channel capacity is a system-level metric. The channel capacity needs to be optimized to achieve maximum possible data throughput to the user terminal. The channel capacity is a function of the signal power, noise level, the number of antennae, and channel that is influenced by antenna and field interactions.

$$C = BW\ log_2\left[\det\left(I_R + \frac{\rho}{N_T} HH^T\right)\right] \quad (1)$$

where, BW = operating bandwidth, $N_R \times N_R$ matrix = arrangements of the receiver antenna, I_R= number of receiver antennas, ρ = signal to noise ratio, N_T = number of transmitting antennas, and HH^T= channel matrix. Higher channel capacity can be achieved by minimizing the port isolation. The field correlation should be minimum so that channel paths are independent to

achieve high channel capacity. The field correlation can be extracted from the impedance matching and s-parameter measurement. It is a challenge to upscale microstrip patch antenna as the radiator into microwave and mm-wave band, Garg, Bhartia, Bahl, and Ittipiboon[3]. While comparing patch antenna with DRA, it has been reported that in patch antenna capacitive effect dominates, which results in a non-spectral wave or ghost wave. It is highly affected by a surface wave and fringing field, whereas DRA is free from it. The patch antenna is affected by mode coupling due to which there will be creations of degenerative modes, whereas DRA is powered by Hybrid LSE and LSM mode. The patch antenna is operated by conduction current whereas, DRA is operated by displacement current, which never leads to ohmic losses. Therefore DRA technology is emerging as a new and viable alternative to conventional low gain and low profile radiating elements. It has huge potential to become the next generation of antenna technology. A DRA is a resonant antenna, fabricated from low-loss microwave dielectric material, the resonant frequency of which is predominantly a function of size, shape, and material permittivity, Petosa, Ittipiboon, Antar, Roscoe and Cuhahi[4]. The impedance bandwidth is a function of the material's permittivity and aspect ratio. The emphasis will be on the compact design of RDRA as a front-end radiating and sensing device to address the needs of portable wireless applications such as PDAs, PCS, WSNs, etc. The aim is to enhance the bandwidth performance to meet the requirements for emerging broadband or ultra-wideband system for high-speed communication. To design a high sensitive and high gain device for commercial sensors, defense, and medical electronics.

In this paper, a modified filleted dual-band dielectric resonator antenna for high-speed applications is proposed, Tripathi, Sahu, Kumari, Parkash, Singh and Kumar[5]. The filleted structure is obtained by placing a half-cut cylindrical dielectric of radius 5 mm made up of low cost and easily accessible dielectric like Alumina with dielectric constant $\varepsilon_r = 9.8$ over a rectangular dielectric with Teflon having $\varepsilon_r = 2.1$. An air gap of height 1 mm is created by placing a foam spacer $\varepsilon_r = 1$ just below the main radiator and above the ground plane. The air gap improves the impedance bandwidth and the impedance matching profile. A slot of dimension 18.9×1.8 mm^2 is created to couple the energy from the micro-strip feed line to the radiator. An infinite ground plane is drawn at the bottom to reduce the front to back ratio to 32.83 dB. A simulation study of the new design was carried out using High-Frequency Structured Simulator Tools (HFSS 14.0), the core of which is derived from the finite element computational technique.

Resonance is said to be a condition in which the field exists without having any excitation. The resonant frequency is never a real number if the radiator is radiating. This multifunctional dual-band antenna resonates within 7.32 GHz to 9.12 GHz and 10.71 GHz to 12.9 GHz with -10 dB impedance fractional bandwidth of 21.92% and 19.09% respectively. The realized radiation efficiency is 96% having a cross-polarization of -20 dB.

The structure of the antenna is presented in Section II. The operating mechanism is described in Section III. The output and input characteristics of the proposed antenna is described in Section IV. Finally, conclusions are made.

2. STRUCTURE OF THE ANTENNA

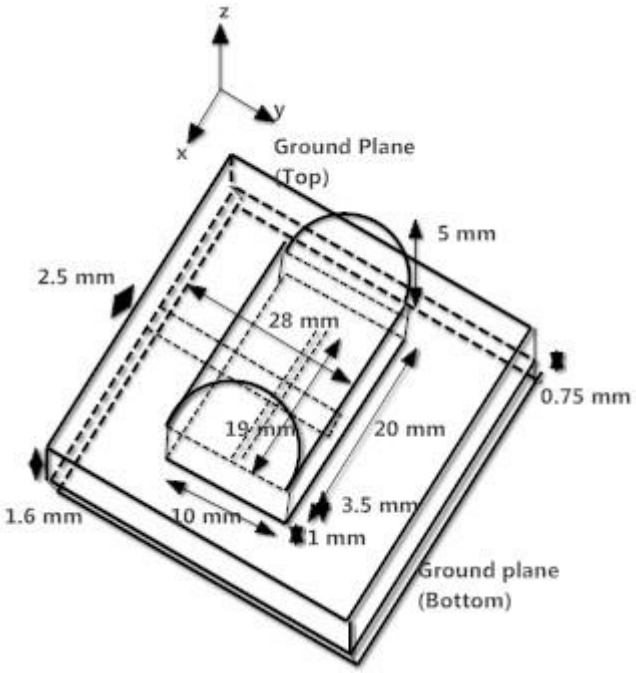

Figure 1. Side view of the proposed radiator

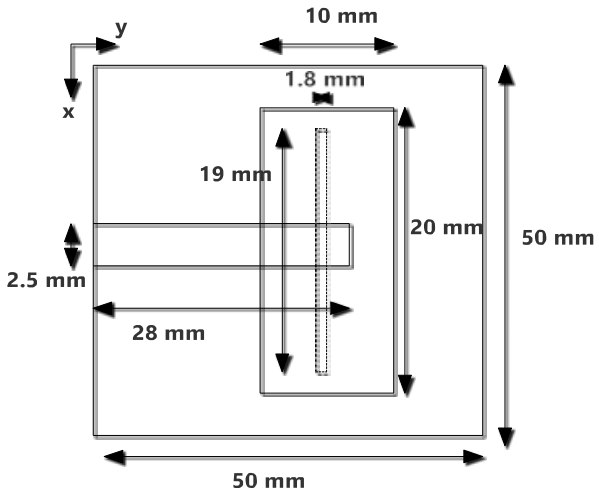

Figure 2. Top view of the antenna

Fig. 1 and 2 show the side view and top view structure of the proposed modified filleted dual-band dielectric resonator antenna. The antenna is placed on a Teflon substrate having $\varepsilon_r = 2.1$ having loss tangent $\tan\delta = 0.001$ with a dimension of 50×50×0.75 mm^3 over which micro-strip line as a feeding transmission line is drawn. Here the quarter-wave transformer is used as an impedance transformer to optimize the matching profile. It is a cascade section of lossless uniform transmission lines or media, each section of which is one-quarter wavelength long at a common frequency. It requires function with flat or equal ripple characteristics in the stopband. The fractional bandwidth can be calculated by, Luk and Leung[6]:

$$W_q = 2\left(\frac{\lambda_{g_1}-\lambda_{g_2}}{\lambda_{g_1}+\lambda_{g_2}}\right) \quad (2)$$

where, $\lambda_{g_1}$and $\lambda_{g_2}$are the longest and shortest guided wavelength. The length of the quarter wave transformer (L) is:

$$L = \frac{\lambda_{g_1}\lambda_{g_2}}{2(\lambda_{g_1}+\lambda_{g_2})} = \frac{\lambda_{g_0}}{4} \quad (3)$$

The dimension of the transmission line, along with the quarter-wave stub, is 2.5×28×0.35 mm^3. The bottom portion of the substrate is covered with a perfect electrical conductor (PEC) as an infinite ground plane. According to the boundary value problem, the field in a region of space is determined from the knowledge of the field over the boundary of the region. The ground plane is a perfectly conducting plane. The boundary condition at PEC has a vanishing tangential component of E (Element source = Image element source) over the plane. It is similar to the solution for a current element adjacent to a plane conductor.

$$n \times H = J_s \quad (4a)$$

$$n \times E = 0 \quad (4b)$$

where, J_s is the source current density. To represent the source, the field equation can be amended to include impressed currents, electric, and magnetic field. This current is the source of the field. The presence of the ground plane below the substrate prevents the deleterious effect of the dielectric constant of the substrate on the bandwidth and scan performance of the radiating structure. It reduces the radiation of energy in an unwanted direction. Because of this, no radiation from the feed network can interfere with the main radiation pattern. Thus large probe self-reactance or wide microstrip lines that are artificial at microwave frequency can be avoided. An aperture of dimension 18.9×1.8 mm^2 is placed at the top ground plane of the upper substrate, which is used to couple energy from the feeding transmission line to the radiator. It is based on the coupling theory, derived from the cavity model. The aperture is acting as an open circuit stub, and it behaves like a magnetic current flowing parallel to the broadside of the slot which, excites the magnetic fields in the DRA. The strongest coupling occurs where the termination of the line is slightly less than one-quarter of a dielectric wavelength from the edge of the dielectric. The transmission line is used to excite the lowest order mode, which will be the dominant mode within the resonator. This slot coupler will act as a major contributor to back radiation. Another substrate (Arlon AD 255 A (tm),$\varepsilon_r = 2.55,\ \tan\partial = 0.0015$) is placed over the bottom substrate to reduce the surface wave, creation of redundant evanescent modes, and to eliminate exposure of field of the microstrip line to the medium of the radiator directly. Therefore, the effect of the feeding mechanisms on the antenna output characteristics can be minimized to a large extent. When the width of the substrate is narrow, it results in high input impedance, much higher than 50Ω, whereas when the width of the substrate is wide, it results in low input impedance of the DRA. So by controlling the width of the substrate, impedance matching can be accomplished. The lower permittivity of the substrate results in increasing the coupling of energy into the DRA. It has been reported that higher bandwidth can be achieved by increasing the substrate thickness or by increasing the size of the radiator. An air gap is introduced at the top of the substrate by placing a thin foam spacer having $\varepsilon_r = 1$ of dimension 50×50×1 mm^3. The air gap is responsible to enhance the resonant frequency and to reduce the radiation Q-factor [6]. Therefore, there is enhancement in the impedance bandwidth and there will be modification of the matching

profile. A rectangular dielectric resonator antenna made up of Teflon having ε_r=2.1, $\tan\delta = 0.001$ of dimension 20×10×3.5 mm^3 is placed over the foam spacer. The shape of the dielectric resonator antenna, its resonant frequency and radiation Q-factor are calculated based on the dielectric wave guide model, Petosa[7]. A half cylindrical structure made up of Alumina Al_2O_3 having ε_r= 9.8, $\tan\delta$ = 0.002) of dimension 20×10 mm^2 cut along XY plane having radius 5 mm is placed over the rectangular structure. The half-cut cylindrical structure is used to increase the effective electrical area of the radiator. The calculation of the resonant frequency of this stacked configuration requires certain adjustments as there is a significant shift in the desired resonant frequency. Therefore, some experimental optimization may be required to maximize the coupling. This top cylindrical structure may be useful in providing high mechanical strength when the antenna will be operated in free space.

The mode within the guide is made up of plane waves reflecting at an angle from the boundaries between dielectric, interfering within the slab to produce different field patterns. The differences are in phases of reflections at the boundaries and in the evanescent field in the dielectric region. If the angle of reflection θ_1 is greater than the critical angle θ_c, where,$\theta_c = \sin^{-1}\left(\frac{\varepsilon_2}{\varepsilon_1}\right)^{\frac{1}{2}}$ then the mode will be confined within the guide. For steeper angle when there is some energy transmission into the outer medium in each reflection leading to leaky wave. Linear combination of Bessel's functions defined this problem along with Hankel's ffunction for the characterization of the wave traveling in the outward direction.

3. PRINCIPLE OF OPERATIONS

The fundamental approach to achieving a wide-band design is to activate different field patterns or modes to initiate different field configurations. Basically, there are three methods to improve

Table 1: Structure of the antenna

Structure	Length	Width	Height	Permittivity	Material	tan δ
Substrate (bottom)	50 mm	50 mm	0.75 mm	2.1	Teflon	0.001
Substrate (top)	50 mm	50 mm	0.75 mm	2.55	Arlon AD 255 A (tm)	0.0015
RDRA	20 mm	10 mm	3.5 mm	2.1	Teflon	0.001
Half Cylindrical DRA	20 mm	10 mm	Radius = 5 mm	9.8	Alumina (Al_2O_3)	0.002

bandwidth. They are (i) impedance matching (ii) use of multiple resonance (iii) use of lossy material. When the thickness of the substrate increases, there will be a decrease in permittivity and capacitance of the dielectric using which bandwidth increases. However, there is a substantial increase in the inductive reactance, which can be nullified by having a suitable impedance matching network. Substrate thicker than a few hundred wavelengths results in spurious radiation from the bend in the microstrip line and face difficulty in impedance matching. Therefore there will be decay in radiation efficiency and pattern degradation. Therefore it is concluded that comparatively thick substrates with a low dielectric constant are preferred for good bandwidth along with appropriate matching technique. Here a stacked configuration results in a thicker dielectric. Further, impedance bandwidth can be increased by the use of two or more staggered tuned resonators with stacked configuration. But this approach does not have a fixed phase center with a frequency that may affect the array design. The slot in the aperture coupling can alter the dimensionality of the boundary value problem and introduce a higher-order mode through the creation of a fringing field. As the slot will operate close to the resonance, bandwidth increases, but it constitutes an increase in back radiation level, which reduces the front-to-back ratio. The front to back ratio is the difference between maximum gains, usually in 0° to that of 180°. The bandwidth can be improved by adding one or more resonant element having a resonating frequency close to one another to achieve multiple resonances. All these points are taken into consideration while placing a half-cut cylinder over the rectangular dielectric. It is supported by a thicker stacked dielectric with a slot. The major attractive feature of this design is to increase the surface area. This structure is somehow similar to the array configuration. The proximity of the stacked structure ensures high coupling.

The bottom dielectric radiator has a rectangular geometry. It is because, in rectangular DRA length, width and depth constitute two degrees of freedom (length/width and depth/width), which provides several aspect ratios and radiation Q-factor for a fixed resonant frequency. Design equations determine the resonant frequency and radiation Q-factor for the fundamental structures. While formulating the design equation, the lowest order modes are considered for the DRA in isolation, and DRA mounted on an infinite ground plane acting as a perfect electrical conductor (PEC) with infinite conductivity. It does not take into account excitation mechanisms, selection, and location of feed networks, coupling coefficient while formulating the design equations. The

excited dominant mode for the lower rectangular DRA is the $TE_{\delta 11}$ mode, which is radiating in the x-direction. Therefore dimension of the rectangular structure plays a significant role in ensuring the mitigation of any unwanted modes especially in the frequency band of operations. The resonant frequency of the bottom rectangular dielectric can be obtained by solving the transcendental equation derived from the dielectric wave guide model, Mongia and Bhartia[8]. The resonant frequency of $TE^{x}{}_{\delta 11}$ can be obtained by solving the transcendental equation.

$$k_x \tan\left(\frac{k_x d}{2}\right) = \sqrt{(\varepsilon_r - 1){k_0}^2 - {k_x}^2} \tag{5}$$

where, $k_0 = \frac{2\pi}{\lambda_0} = \frac{2\pi f_0}{c}, k_y = \frac{\pi}{w}, k_z = \frac{\pi}{b}$

$$ {k_x}^2 + {k_y}^2 + {k_z}^2 = \varepsilon_r {k_0}^2 \tag{6}$$

The transcendental equation can be solved for selected ratio of w/b as a function of d/b w.r.t normalized frequency F. The normalized frequency F can be defined as

$$F = \frac{2\pi w f_0 \sqrt{\varepsilon_r}}{c} \tag{7}$$

Here f_0 is the resonant frequency. The value of the normalized frequency F can be determined from the F vs. (d/b) plot for different value of (w/b). The above equation can be effectively written as

$$f_{GHz} = \frac{15F}{w_{cm}\pi\sqrt{\varepsilon_r}} \tag{8}$$

where, resonant frequency is represented in GHz scale and w is in cm. At the top of the rectangular DRA, a filleted structure is being embedded, which is excited with a hybrid field pattern. The top cylindrical shape is characterized by radius ‘a’ and height ‘h’, which provides one degree of freedom with an aspect ratio of a/h. The aspect ratio decides the $k_0 a$ and the radiation Q-factor for a particular dielectric constant, “Long, McAllister and Shen[9]. The approximate calculated value of the resonant frequency and radiation Q-factor for the hybrid lower order modes$HE_{11\delta}$, when DRA is in a state of isolation without having ground plane is:

$$k_0 a = \frac{6.324}{\sqrt{\varepsilon_r + 2}}\left\{0.27 + 0.36\frac{a}{2h} - 0.00898\left(\frac{a}{2h}\right)^2\right\} \tag{9}$$

$$Q = 0.0107{\varepsilon_r}^{1.3}\frac{a}{h}\left\{1 + 100e^{-2.05\left(\frac{a}{2h} - \frac{1}{80}\left(\frac{a}{h}\right)^2\right)}\right\} \tag{10}$$

Though the above equations are not quite accurate, they are accurate enough to show the initial

direction later design can be concretized through adopting different matching profiles and coupling mechanisms.

At the boundary between the two structure mode conversion takes place and the dominant mode becomes hybrid$HE_{11\delta}$. The overall field pattern within the device is the contribution of the ground plane, microstrip transmission line, quarter-wave stub, air gap, aperture, a stacked combination of lower rectangular and upper filleted dielectric resonator. These factors, when combined with an isolated DRA structure will load the antenna and shift the calculated resonant frequency, radiation Q-factor and radiation characteristics mainly cross-polarization levels. Detail knowledge of the internal field structure and the coupling coefficient is mandatory to characterize the antenna. So the overall performance of a DRA depends upon generated modes, amount of coupling, and frequency response of the impedance. These quantities are difficult to determine without using any numerical techniques, Garg[10].

The radiation field pattern of $HE_{11\delta}$ mode is similar to a short horizontal magnetic dipole. Due to system complexities there are no concrete solutions of the field patterns of a cylindrical dielectric resonator antenna. Magnetic wall boundary condition is suitable for the approximate calculation of the field at different points in space.

The point of excitation is said to be a sensitive point. The power will be real above the cutoff and imaginary below the cutoff. So we need to nullify the imaginary part by placing the source at the point of (i) maximum electric field (at λ/4) (ii) polarization matching (iii) 50Ω impedance matching (iv) minimum mode coupling & mode degeneracy. In the presence of the source, DRA can be characterized by Helmholtz's equation. Helmholtz's equation is the sun in electromagnetic from which electric and magnetic fields can be calculated from the electric and magnetic current density by taking the route of potential functions. The potential function can be calculated through scalar manipulations so that we can avoid complicated vector manipulation. Electric and magnetic vector potentials are man-made quantities, Huang and Boyle[11].

$$\nabla^2 A + k^2 A = -J \tag{11}$$

$$\nabla^2 F + k^2 F = -M \tag{12}$$

where, F= Electric vector potential, A= Magnetic vector potential. The most common technique to analyze the DRA is the Finite element method. The main aim of the analysis is to find the electric and magnetic field with high accuracy when charge distribution and flow of current is

given. The FEM contains features like geometrical adaptability and is a convenient time-domain technique for transient analysis. It describes irregular boundaries and non-homogeneous material properties of the radiator and feeding mechanisms. The unique advantage of the FEM is that it does not require the formulation of equivalent current, and it does not allow the field to discretize and disperse. It helps to reduce the dimensionality of the problem by resolving the 3D problem by using a 2D approach. Therefore, an arbitrary structure can be better tracked and shaped with high accuracy while reducing the cost of the computation. DRA and its entire volume, surroundings can be discretized to increase the computational size of the problem. Here High-frequency structured simulator (HFSS) is used to calculate field intensity, potential difference, energy, and current densities for the design of high frequency and high-speed devices.

4. Input and Output Characteristics of the Proposed Antenna

Bode showed that the most important limitation of broadband impedance matching of loads is the reactive element and resistor connected in series and parallel to the network. Later Fano showed that the efficiency of signal transmission and channel bandwidth are exchangeable quantities in the process of impedance matching of the reactive component, Matthaei, Young and Jones [12]. Reflection coefficient (S11) corresponds to the input impedance and can be defined as the ratio of reflected wave phasor to the incident wave phasor. S parameter describes wave propagation within the device and is a function of number of ports and the operating frequency. As shown in Fig 3 the return loss versus frequency graph, the resonating frequency below -10dB comes out to be 8.21 GHz from 7.32 GHz to 9.12 GHz and 11.73 GHz from 10.71 GHz to 12.95 GHz. However, practically it has been observed that less than -8dB the antenna will function quite well. The impedance bandwidth for Band-I is found to be 21.92% and impedance bandwidth for Band-II is found to be 19.09%. This dual wideband response covers the frequency from 3.1 GHz to 10.6 GHz. This embedded stacked configuration is very sensitive to variation in frequency response. Fig 4 describes the impedance smith chart, which provides polar form of mapping of the impedance plane and the reflection coefficient. At 8.21 GHz and 11.73 GHz a perfect match is plotted and is a vector of zero length i.e. 1+j0 or 50 Ω.

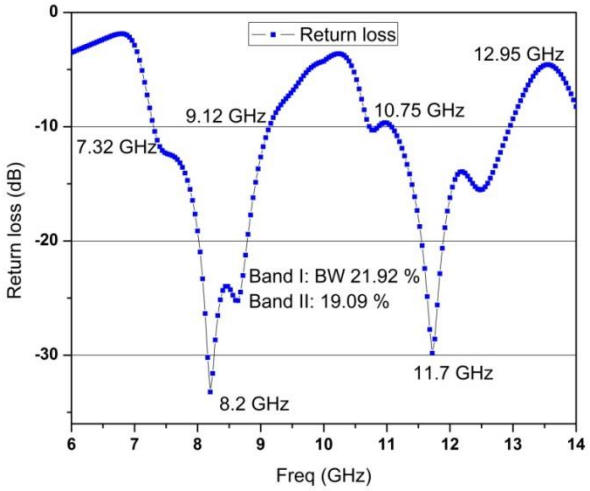

Fig. 3: Plot of return loss versus frequency

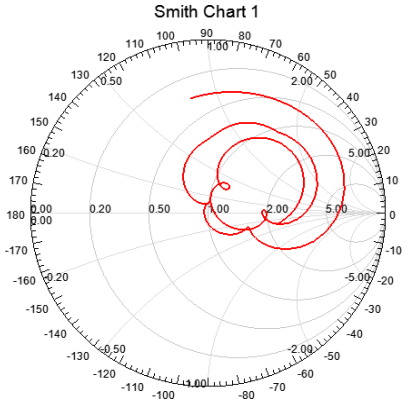

Fig. 4: The Impedance smith chart

Fig. 5 and 6 shows the output radiated electric and magnetic field in the xz and yz plane at $\emptyset = 0°$ and $\emptyset = 90°$ at 7 GHz. The radiation plot guides how to aim the antenna towards its corresponding receiver. The half power beam width or 3 dB beam width is the point between which half of the power is concentrated. Here the half power beam width is found to be 70°. From this output characteristic graph, it is found that radiation is basically concentrated in the broadside direction with $\theta = 0°$. Though high conductivity infinite ground is placed at the bottom of the antenna but still it is found that there is considerable back radiation with front to back ratio of around -30 dB. It means power is mainly concentrated in the main lobe and low power is being wasted in the back lobe of the radiator, Mohanty and Mohapatra [13]. Further the radiation pattern is found to be symmetric along the z-axis.

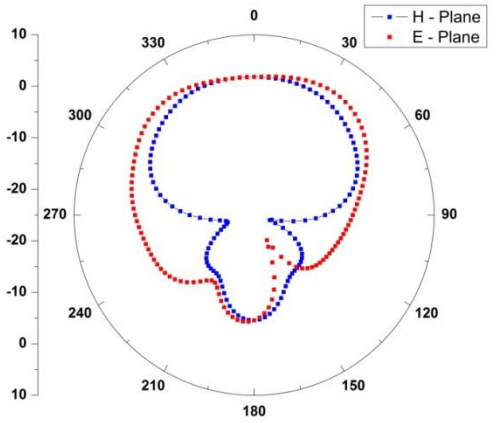

Fig. 5: Radiation pattern of the antenna in the E and H plane (10dB/div)

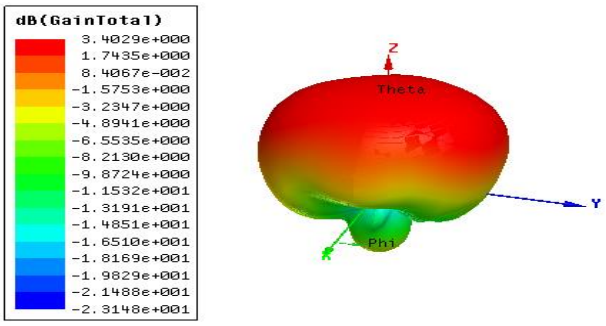

Fig. 6: 3 D radiation pattern of the proposed antenna

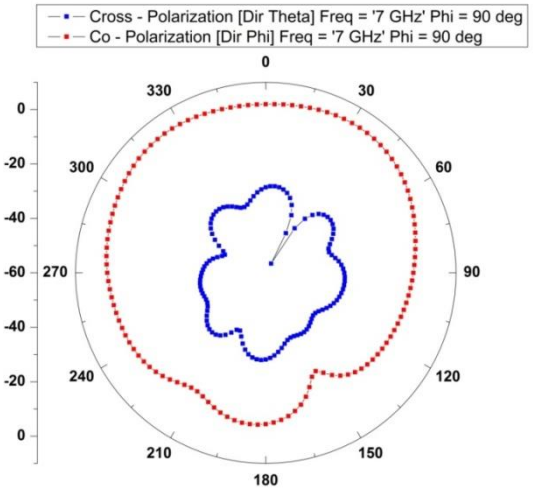

Fig. 7: Radiation pattern indicating E-plane co and cross polarization of the antenna (10 dB/div)

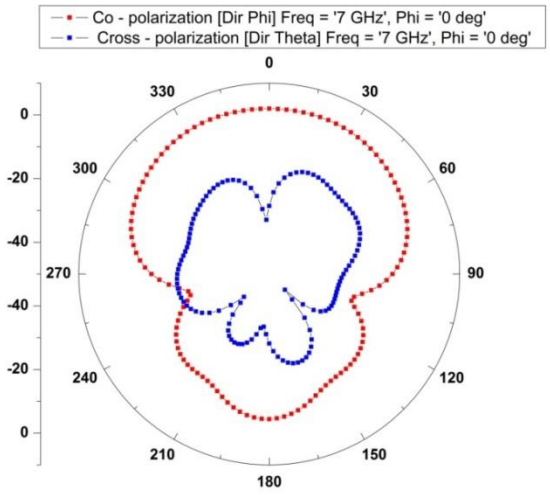

Fig. 8: Radiation pattern indicating E-plane co and cross polarization of the antenna (10 dB/div)

Fig 7 & 8 show the Co and Cross polarization in the electric and magnetic plane. This co and cross-polarization indicate the electric and magnetic field between the transmitting and receiving platform. The cross-polarization is around 28 dB lesser than the co polarization for the electric plane and around 25 dB lesser for the magnetic plane. Commercial antenna technology demands a co and cross-polarization difference of around 20 dB for effective noiseless communication, Diao, Su, Liu, Li and Wang [14]. This parameter plays a significant role in near field ultra-wideband communication where transmission range is relatively poor due to low transmitted power.

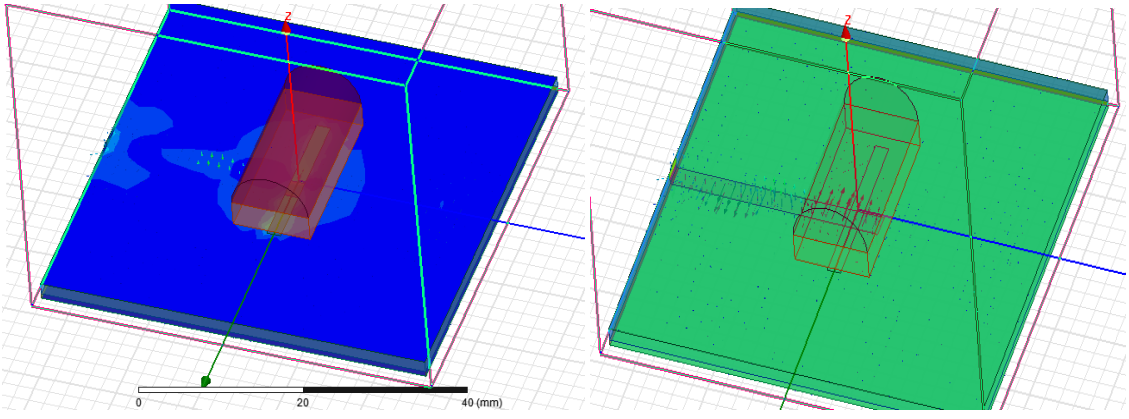

Fig. 9: The current density and electromagnetic field in the proposed radiator

DRA technology is still in its early stages of development, and more research is required to overcome some of the challenges associated with fabricating a large number of DRA elements and assembling them into an array. A wide variety of dielectric material is available based on its mechanical, electrical, and thermal properties. In the millimeter and microwave frequency, the operation tolerance control of the dielectric material is the most tedious, which leads to the difficulty to achieve high design accuracy. DRA uses an insufficient and un-matured numerical technique for its performance analysis (especially Rectangular DRA). It is required to improve RDRA's mathematical modeling to analyze its design characteristics. Hybrid DRA with active switching elements can be useful for beamforming and beam splitting techniques, Ali, Jamaluddin, Gaya and Rahim [15].

5.CONCLUSION

Wireless near field ultra-wideband communication has been undergoing tremendous growth in recent time due to the expansion of technologies like Internet of Thing (IoT), Blue tooth, Wireless Local Loop (WLL), Wireless Fidelity (Wi-Fi), Local Multipoint Distributive System (LMDS), which mainly concentrate in the range of 3.1 GHz to 10.6 GHz and expanded up to X-band range. This multifunctional dual-band antenna resonates within 7.32 GHz to 9.12 GHz and 10.71 GHz to 12.9 GHz with -10 dB impedance fractional bandwidth of 21.92% and 19.09% respectively. Though due to a double infinite ground plane this structure is somehow bulky but its electrical characteristics are found to be very robust. This antenna is suitable for modern high-speed ultra wideband internet of things and enhanced mobile broadband applications.

CONFLICT OF INTERESTS

The author(s) declare that there is no conflict of interests.

REFERENCES

[1] J.D. Kraus, D.A. Fleisch, Electromagnetics with applications, Tata McGraw-Hill, New Delhi, (2010).

[2] R.F. Harrington, Time-harmonic electromagnetic fields, IEEE Press: Wiley-Interscience, New York, 2001.

[3] R. Garg, P. Bhartia, I. Bahl, A. Ittipiboon, Microstrip antenna design handbook, Artech House, Norwood, 2001.

[4] A. Petosa, A. Ittipiboon, Y.M.M. Antar, D. Roscoe, M. Cuhaci, Recent advances in dielectric-resonator antenna technology, IEEE Antennas Propag. Mag. 40 (1998), 35–48.

[5] P. Tripathi, B. Sahu, P. Kumari, O. Parkash, S.P. Singh, D. Kumar, Filleted rectangular dielectric resonator antenna using BST ceramic with improved bandwidth, in: 2015 IEEE Applied Electromagnetics Conference (AEMC), IEEE, Guwahati, India, 2015: pp. 1–2.

[6] K.M. Luk, K.W. Leung, Dielectric Resonator Antennas, Research Studies Press, Chichester, 2003.

[7] A. Petosa, Dielectric resonator antenna handbook, Artech House, Boston, 2007.

[8] R.K. Mongia, P. Bhartia, Dielectric resonator antennas—a review and general design relations for resonant frequency and bandwidth, Int. J. Microw. Mill.-Wave Comput.-Aided Eng. 4 (1994), 230–247.

[9] S. Long, M. McAllister, Liang Shen, The resonant cylindrical dielectric cavity antenna, IEEE Trans. Antennas Propagat. 31 (1983), 406–412.

[10] R Garg, Analytical and computational methods in electromagnetics, Artech House, Norwood, 2008.

[11] Y. Huang, K. Boyle, Antenna from Theory to Practice, John Wiley and Sons Ltd, (2008).

[12] G. Matthaei, L. Young, E.M.T. Jones, Microwave filters, impedance-matching networks, and coupling structures, Artech House, Norwood, Massachusetts, 1980.

[13] S. Mohanty, B. Mohapatra, Leaky Wave-Guide Based Dielectric Resonator Antenna for Millimeter-Wave Applications, Trans. Electr. Electron. Mater. (2020). https://doi.org/10.1007/s42341-020-00240-w.

[14] Y. Diao, M. Su, Y. Liu, S. Li, W. Wang, Compact and multiband dielectric resonator antenna for mobile terminals, in: 2015 IEEE International Symposium on Antennas and Propagation & USNC/URSI National Radio Science Meeting, IEEE, Vancouver, BC, Canada, 2015: pp. 1724–1725.

[15] I. Ali, M.H. Jamaluddin, A. Gaya, H.A. Rahim, A dielectric resonator antenna with enhanced gain and bandwidth for 5G applications, Sensors. 20 (2020), 675.